ORIGINAL ARTICLE

Numerical simulation of mixed convection heat transfer of nanofluid in a double lid-driven cavity using lattice Boltzmann method

CrossMark

Ahmad Reza Rahmati *, **Ali Rayat Roknabadi, Mahmoud Abbaszadeh**

Department of Mechanical Engineering, Faculty of Engineering, University of Kashan, Iran

Abstract   In this study, mixed convection heat transfer of water-Cu nanofluid in a double lid-driven cavity has been analyzed by lattice Boltzmann method. The double lid-driven are insulated and the side walls have sinusoidal temperature distribution. Simulations have been carried out at constant Grashof number 100, the Richardson numbers of 0.01, 0.1,1,10 and 100, temperature phase deviation of 0, $\pi/4$, $\pi/2$, $3\pi/4$ and π, the solid volume fraction from zero to 0.06 and the Prandtl number of 6.57. The thermal modeling of passive scalar is applied and two separate distribution functions for the flow and temperature fields are considered. In order to calculate the thermal conductivity coefficient of nanofluid, constant and variable properties models are used. The results showed that in high Richardson numbers, the effect of the thermal phase deviation changes on the flow pattern is evident and in low Richardson numbers, the phase deviation changes do not affect the flow pattern. In all thermal phase deviations by reducing the Richardson number, the Nusselt number increases and thus the heat transfer increases. Also the average Nusselt number obtained for the constant properties model is higher compared with that of variable properties model.

1. Introduction

Fluid flow and heat transfer in a cavity which is driven by buoyancy and shear force are discussed in variety of thermal engineering applications such as food processing and float glass production, solar collectors, lake and reservoirs, nuclear reactors, solar ponds and crystal growth [1–12]. Interaction of

buoyancy force due to temperature gradient with forced convection due to shear forces is a complex phenomenon called mixed convection. Numerous researches have been published in this type of problem such as the single or double lid-driven cavity flow and heat transfer involving different cavity configurations, various fluids and imposed temperature gradients in the last two decades. For example, Sharif [13] studied laminar mixed convection in a shallow inclined cavity where the top wall is warm and the bottom wall is cool. He indicated that the average Nusselt number increases by increasing cavity inclination angle for forced convection-dominated regime ($Ri = 0.1$) while it increases more rapidly for natural

convection-dominated regime (Ri = 10). Tiwari and Das [14] numerically investigated the mixed convection heat transfer and fluid flow of Cu–water nanofluid in a square cavity with top and bottom insulated walls and differentially-heated moving sidewalls. They found that when the Ri = 1, the average Nusselt number increases substantially with augmentation of the volume fraction of the nanoparticles. Muthtamilselvan et al. [15] numerically examined the mixed convection flow and heat transfer of Cu–water nanofluid in a lid-driven rectangular enclosure. The sidewalls of the enclosure were adiabatic while the horizontal walls were kept at constant temperatures and the top wall moved at a constant velocity. Arefmanesh and Mahmoodi [16] performed a numerical study to examine the effects of uncertainties of viscosity models for the Al_2O_3–water nanofluid on mixed convection in a square cavity with cold left, right, and top walls and moving bottom hot wall. Their results showed that the average Nusselt number of the hot wall increases by increasing the volume fraction of nanoparticles for both viscosity models which are used. Mazrouei Sebdani et al. [17] conducted a numerical simulation to investigate effect of nanofluid variable properties on mixed convection in a square cavity with moving cold side walls and a constant temperature heater on the bottom wall. Their results showed that the heat transfer of the nanofluid could be either enhanced or alleviated with respect to the base fluid which depends on the Reynolds number and Rayleigh number. The other applications of the mixed convection can be found in Ref. [18–36].

Numerical methods in the recent years have a lot of advantages in solving the heat transfer and fluid flow equations. One of these methods that grows rapidly and has a widespread application in industry is lattice Boltzmann method. Nemati et al. [37] have examined the mixed convection heat transfer in a lid-driven cavity using Lattice Boltzmann simulation. They showed that by increasing the volume fraction of nanofluid, heat transfer rate increases and this augmentation is more for Cu, CuO and Al_2O_3 nanofluids, respectively. Rabienatajdarzi et al. [38] simulated mixed convection heat transfer in a lid-driven square inclined cavity in different inclination angles by using the lattice Boltzmann method. The vertical walls of the cavity are insulated, while the bottom wall is warm and upper wall is cold and is kept at a uniform temperature. Their results showed that the heat transfer rate is independent of the tilt angle for the Richardson number 0.01 and when the Richardson number increases, heat transfer rate also varies. Karimpour et al. [39] investigated the laminar mixed convection heat transfer in a lid-driven rectangular enclosure by use of the lattice Boltzmann method. They applied double distribution function thermal model in various Richardson numbers, tilt angles and Prandtl numbers. According to their results, when the Prandtl number increases, the heat transfer rate increases too. Other researches in the field of lattice Boltzmann method are presented in [40–45].

Considering the previous studies, it is clear that no research is conducted in the field of mixed convection heat transfer in double lid-driven cavities with sinusoidal temperature distribution on sidewalls by use of the lattice Boltzmann method. In this study, by considering a square cavity, the effect of the Richardson number, the type and concentration of nanoparticles and sinusoidal temperature phase change on the heat transfer and flow field are examined. Also by adding nanofluids, a comparison between the two models, constant properties and variables properties, is done.

2. The governing equations and boundary conditions

Fig. 1 shows the studied geometry with the boundary conditions. The square cavity has double lid-driven and insulated and the side walls have sinusoidal temperature distribution and the right side wall has a temperature phase deviation. The cavity is filled with water-Cu nanofluid. Thermophysical properties of water as a base fluid and Cu nanoparticles are presented in Table 1.

Before introducing the governing equations, the following dimensionless parameters are defined:

$$X = \frac{x}{H}, \quad Y = \frac{y}{H}, \quad U = \frac{u}{U_0}, \quad V = \frac{v}{U_0}, \quad \theta = \frac{T - T_C}{T_h - T_C},$$
$$P = \frac{p}{\rho_{nf}U_0^2} \tag{1}$$

Based on the above dimensionless parameters, the dimensionless governing equations including conservation of mass, momentum conservation in x and y directions and energy conservation for a two dimensional, laminar and steady flow are as follows:

$$\frac{\partial U}{\partial x} + \frac{\partial V}{\partial y} = 0 \tag{2}$$

$$U\frac{\partial U}{\partial X} + V\frac{\partial U}{\partial Y} = -\frac{\partial P}{\partial X} + \frac{1}{Re}\frac{\mu_{eff}}{v_f\rho_{nf}}\left(\frac{\partial^2 U}{\partial X^2} + \frac{\partial^2 U}{\partial Y^2}\right) \tag{3}$$

$$U\frac{\partial V}{\partial X} + V\frac{\partial V}{\partial Y} = -\frac{\partial P}{\partial Y} + \frac{1}{Re}\frac{\mu_{eff}}{v_f\rho_{nf}}\left(\frac{\partial^2 V}{\partial X^2} + \frac{\partial^2 V}{\partial Y^2}\right) + \frac{(\rho\beta)_{nf}}{\rho_{nf}\beta_f}Ri\theta \tag{4}$$

$$U\frac{\partial \theta}{\partial X} + V\frac{\partial \theta}{\partial Y} = \frac{\alpha_{nf}}{\alpha_f}\frac{1}{PrRe}\left(\frac{\partial^2 \theta}{\partial X^2} + \frac{\partial^2 \theta}{\partial Y^2}\right) \tag{5}$$

where Re is Reynolds number, defined as $\frac{u\,H}{v_f}$ and quantifies the relative importance of inertial forces to viscous forces. Ri is Richardson number, expressed as $\frac{g\beta\Delta TH}{u^2}$ and represents the importance of natural convection relative to the forced convection. Pr is Prandtl number, given as $\frac{v_f}{\alpha_f}$.
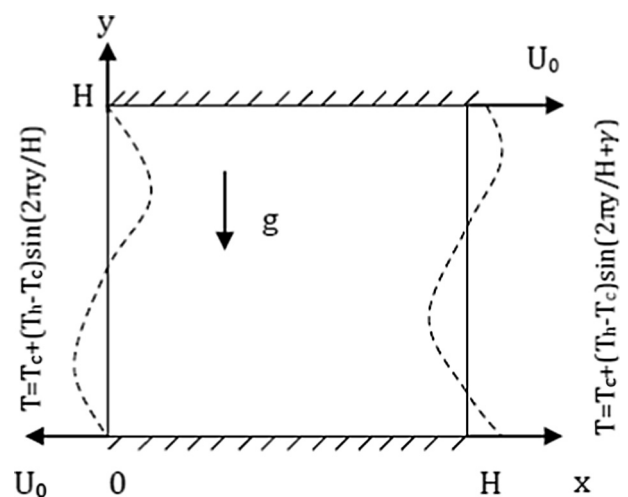

Figure 1 Schematic view and boundary conditions of the problem.

Table 1 Thermo-physical properties of the base fluid and nanoparticles [46].

Thermo-physical properties	Water	Cu
$\beta \times 10^{-5}$ (1/k)	21	1.67
k (W/m K)	0.613	400
c_p (J/kg K)	4179	383
ρ (kg/m^3)	997.1	8954
$\mu \times 10^{-4}$ (kg/m s)	8.55	–

With regard to the geometry of the problem, the dimensionless boundary conditions are as follows:

On the bottom wall of the cavity	$U = -1$, $V = 0$, $\frac{\partial \theta}{\partial n} = 0$
On the top wall of the cavity	$U = 1$, $V = 0$, $\frac{\partial \theta}{\partial n} = 0$
On the left side wall of the cavity	$U = V = 0$, $\theta = \sin(2\pi Y)$
On the right side wall of the cavity	$U = V = 0$, $\theta = \sin(2\pi YH/H + \gamma)$

Nanofluid properties such as density, heat capacity, volume expansion coefficient, diffusion coefficient, effective dynamic viscosity and thermal conductivity coefficient [47,48], are obtained from the relations 6 to 11, respectively.

$$\rho_{nf} = (1 - \varphi)\rho_f + \varphi\rho_p \tag{6}$$

$$(\rho c_p)_{nf} = (1 - \varphi)(\rho c_p)_f + \varphi(\rho c_p)_p \tag{7}$$

$$(\rho\beta)_{nf} = (1 - \varphi)(\rho\beta)_f + \varphi(\rho\beta)_p \tag{8}$$

$$\alpha_{nf} = \frac{k_{nf}}{(\rho c_p)_{nf}} \tag{9}$$

$$\mu_{nf} = \frac{\mu_f}{(1 - \varphi)^{2.5}} \tag{10}$$

$$\frac{k_{nf}}{k_f} = \frac{(k_p + 2k_f) - 2\varphi(k_f - k_p)}{(k_p + 2k_f) + \varphi(k_f - k_p)} \tag{11}$$

Thermal conductivity coefficient of nanofluids for variable properties model is [49]:

$$k_{nf} = k_f\left[1 + \frac{k_p A_p}{k_f A_f} + ck_p pe\frac{A_p}{k_f A_f}\right], \quad \frac{A_p}{A_f} = \frac{d_f}{d_p}\frac{\varphi}{1 - \varphi}$$
$$Pe = \frac{u_p d_p}{\alpha_f}, \quad u_p = \frac{2k_B T}{\pi\mu_f d_p^2}, \quad k_B = 1.3807 \times 10^{-23} \text{ J K}^{-1} \tag{12}$$

c is the experiment constant that for water-Cu nanofluids used in the present work is obtained 36,000. d_f, and d_p are the diameter of water molecules and Cu particles and equal to 2×10^{-10} and 100×10^{-10}, respectively. u_p is Brownian motion speed.

3. Numerical simulation

3.1. Lattice-Boltzmann method

The Boltzmann equation consists of two parts: distribution and collision. In the distribution step, the distribution functions proceed in their velocity direction to the adjacent nodes and the collision step represents particle collision with each other at each node in a way that the conservation of mass, momentum and energy laws is satisfied (Fig. 2). In the present

work, the two-dimensional grid model or the so-called D$_2$Q$_9$ grid is used for both stream function and temperature [50].

In the present study, the passive scalar heating model is used in the lattice Boltzmann method. In this model, the two separate distribution functions are used for flow and temperature fields. f and g are the distribution functions for the flow field and temperature, respectively. The f distribution function is used for calculating density and velocity field and the g distribution function is used for calculating temperature field.

The governing equations in the lattice Boltzmann method for flow and temperature distribution function are as follows:

$$f_i(\mathbf{x} + \mathbf{c}_i\Delta t, t + \Delta t) - f_i(\mathbf{x}, t) = -\frac{\Delta t}{\tau_v}[f_i(\mathbf{x}, t) - f_i^{eq}(\mathbf{x}, t)] + \Delta t\, \mathbf{c}_i \cdot \mathbf{F} \tag{13}$$

$$g_i(\mathbf{x} + \mathbf{c}_i\Delta t, t + \Delta t) - g_i(\mathbf{x}, t) = -\frac{\Delta t}{\tau_c}[g_i(\mathbf{x}, t) - g_i^{eq}(\mathbf{x}, t)] \tag{14}$$

c_i, and Δt represent the discrete velocity vector and grid time step, respectively. τ_c, and τ_v represent the relaxation times related to the flow and temperature field. f_i^{eq}, and g_i^{eq} indicate the local equilibrium distribution functions which are calculated for the flow and temperature fields as follows [37]:

$$f_i^{eq}(\mathbf{x}, t) = \omega_i\rho\left[1 + \frac{\mathbf{c}_i \cdot \mathbf{u}}{\mathbf{c}_s^2} + \frac{1}{2}\frac{(\mathbf{c}_i \cdot \mathbf{u})^2}{\mathbf{c}_s^4} - \frac{1}{2}\frac{\mathbf{u} \cdot \mathbf{u}}{\mathbf{c}_s^2}\right] \tag{15}$$

$$g_i^{eq} = \omega_i T\left[1 + \frac{\mathbf{c}_i \cdot \mathbf{u}}{\mathbf{c}_s^2}\right] \tag{16}$$

where ρ, T and $\mathbf{u}$ are the density, temperature and macroscopic velocity vector, respectively and the weight functions ω_i for the D$_2$Q$_9$ model are $\omega_0 = 4/9$, $\omega_{1-4} = 1/9$ and $\omega_{5-8} = 1/36$.

c_s is the sound speed and equal to $c/\sqrt{3}$, and $c = \frac{\Delta x}{\Delta t} = \frac{\Delta y}{\Delta t}$. Discrete grid velocity c_i for the D$_2$Q$_9$ model is defined as follows:

$$c_i = \begin{cases} 0 & i = 0 \\ c(\cos[(i-1)\pi/2], \sin[(i-1)\pi/2]) & i = 1-4 \\ c\sqrt{2}(\cos[(i-5)\pi/2 + \pi/4], \sin[(i-5)\pi/2 + \pi/4]) & i = 5-8 \end{cases} \tag{17}$$

By using the expansion of Chapman-Enskog, the Navier-Stokes equations can be derived from the proposed model. With this expansion, the kinematic viscosity and thermal diffusivity coefficient are expressed as follows:

$$\upsilon = \left[\tau_v - \frac{1}{2}\right]c_s^2\Delta t, \quad \alpha = \left[\tau_c - \frac{1}{2}\right]c_s^2\Delta t \tag{18}$$

In this study, the Boussinesq approximation is applied for the buoyancy force. The buoyancy force in vertical direction is as follows:

$$F_i = 3\omega_i\rho g_y\beta\Delta T \tag{19}$$

In order to ensure that the simulation occurs near incompressible regime, the characteristic velocity of the flow for both natural, $V_{natural} = \sqrt{g\beta\Delta TH}$, and force, $V_{force} = Re\upsilon/H$, regimes must be smaller than the fluid speed of sound. In the present study, the characteristic velocity was selected as 0.1 of sound speed.

The macroscopic quantities such as density, temperature and velocity vector are calculated by using the following relations:
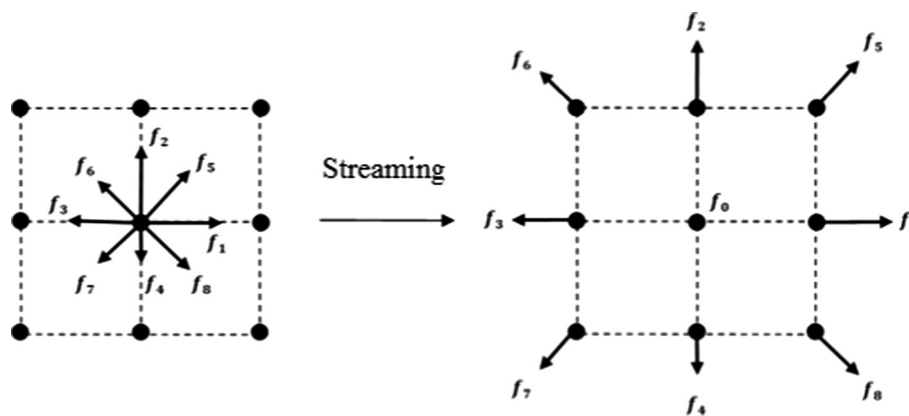
Figure 2 The distribution step for D_2Q_9 model.

$$\rho = \sum_i f_i \tag{20}$$

$$\rho\mathbf{u} = \sum_i f_i \mathbf{c}_i \tag{21}$$

$$T = \sum_i g_i \tag{22}$$

$$\sqrt{\frac{1}{N'}\sum\left(U^{n'+1} - U^{n'}\right)^2 + \left(V^{n'+1} - V^{n'}\right)^2} \leqslant 10^{-6} \tag{23}$$

$$\sqrt{\frac{1}{N'}\sum\left(\theta^{n'+1} - \theta^{n'}\right)^2} \leqslant 10^{-6} \tag{24}$$

3.2. Independence results from grid

To find a suitable grid that leads to the autonomous results from grid and in order to determine the appropriate grid size, the average Nusselt number of water-Cu nanofluid in the cavity with various grid point numbers for $Ri = 0.1$, $\varphi = 0.04$ and $\gamma = \pi/2$ is presented in Table 2. As can be seen, the discrepancy of the average Nusselt number between the grid with 120×120 points and the grid with 100×100 points is about 0.012%. So the grid with the 100×100 points is selected as the optimal grid.

3.3. Validation of results

In order to validate the computer program results, the problem geometry of Sivasankaran et al. [51] and Abu-Nada and Chamkha [52] with our program is simulated and the results are compared in the form of temperature and flow field and the average Nusselt number in Figs. 3 and 4 and Table 3, respectively. As can be seen in these figures and tables, a good conformity is obtained with the present work.

It is also important to mention that the convergence criteria for velocity and temperature are calculated by Eqs. (23) and (24).

Table 2 The average Nusselt number on the hot wall for water-Cu nanofluid in $Ri = 0.1$, $\varphi = 0.04$ and $\gamma = \pi/2$.

Number of points	Nu_{Avg}
20×20	7.196
40×40	7.930
60×60	8.055
80×80	8.085
100×100	8.088
120×120	8.089

4. Results and discussion

In this section, the results such as the stream lines, the isotherm lines, the local and average Nusselt number diagrams, the velocity and temperature diagrams in the middle of the cavity and comparing the average Nusselt number for two models of nanofluids, constant and variable properties in terms of parameters such as the Richardson number, Grashof number, Reynolds number, volume fraction, and sinusoidal phase change temperature are presented and discussed.

4.1. Study of the flow and temperature field

In Figs. 5 and 6 the stream lines and isotherm lines in constant Grashof number 100, the Richardson numbers 0.01, 0.1, 1, 10 and 100, and the temperature phase deviation $\gamma = 0$, $\gamma = \pi/2$ and $\gamma = \pi$ are indicated. Since the Richardson number in mixed convection represents the amount of the influence of the natural convection to the forced convection, by reducing the Richardson number in constant Grashof number, the Reynolds number increases and the forced convection overcomes natural convection. As seen in Fig. 5 in low Richardson numbers due to the forced convection overcome natural convection, the temperature phase deviation change has no effect on the flow pattern. In $\gamma = 0$ and in high Richardson numbers, stream lines in the center of the cavity are as a circulation which is stretched in vertical direction due to forced convection have more effect than the natural convection. By increasing the Reynolds number, the speed of the top and bottom walls is increased and the flow of nanofluids is more stretched horizontally and circulation strength increases. The stream lines for all Richardson numbers near the top and bottom walls are denser due to the faster flow velocity in these areas.

In Fig. 6, by reducing the Richardson number for all temperature phase deviations and in constant Grashof number, heat transfer increases. Also for the proposed phase deviation, the temperature gradient of pure fluid is steeper than nanoflu-
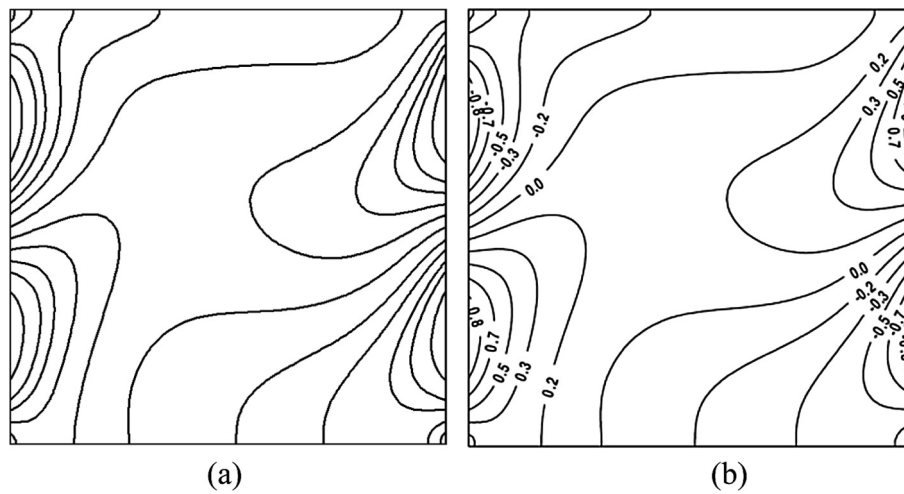
Figure 3   The isothermal lines for (a) present study, (b) Sivasankaran et al. [51] in $Pr = 0.71$ and $Ri = 1$ and $\gamma = \pi$.
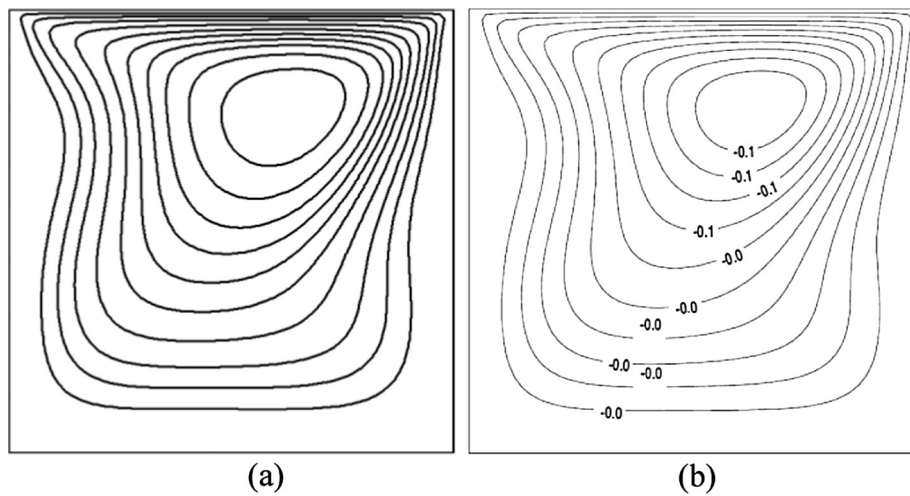

Figure 4   The streamlines for (a) present study, (b) Sivasankaran et al. [51] in $Pr = 0.71$ and $Ri = 1$ and $\gamma = \pi$.

Table 3   Comparing the average Nusselt number in $Gr = 100$ and $\varphi = 0.05$.

Ri	Present study	Abu-Nada and Chamkha [52]	Difference percent
0.2	2.726	2.866	4.8
0.5	2.284	2.365	3.4
2	1.696	1.741	2.5
5	1.425	1.453	1.9

ids along the side walls due to augmentation of the volume fraction of the nanofluids.

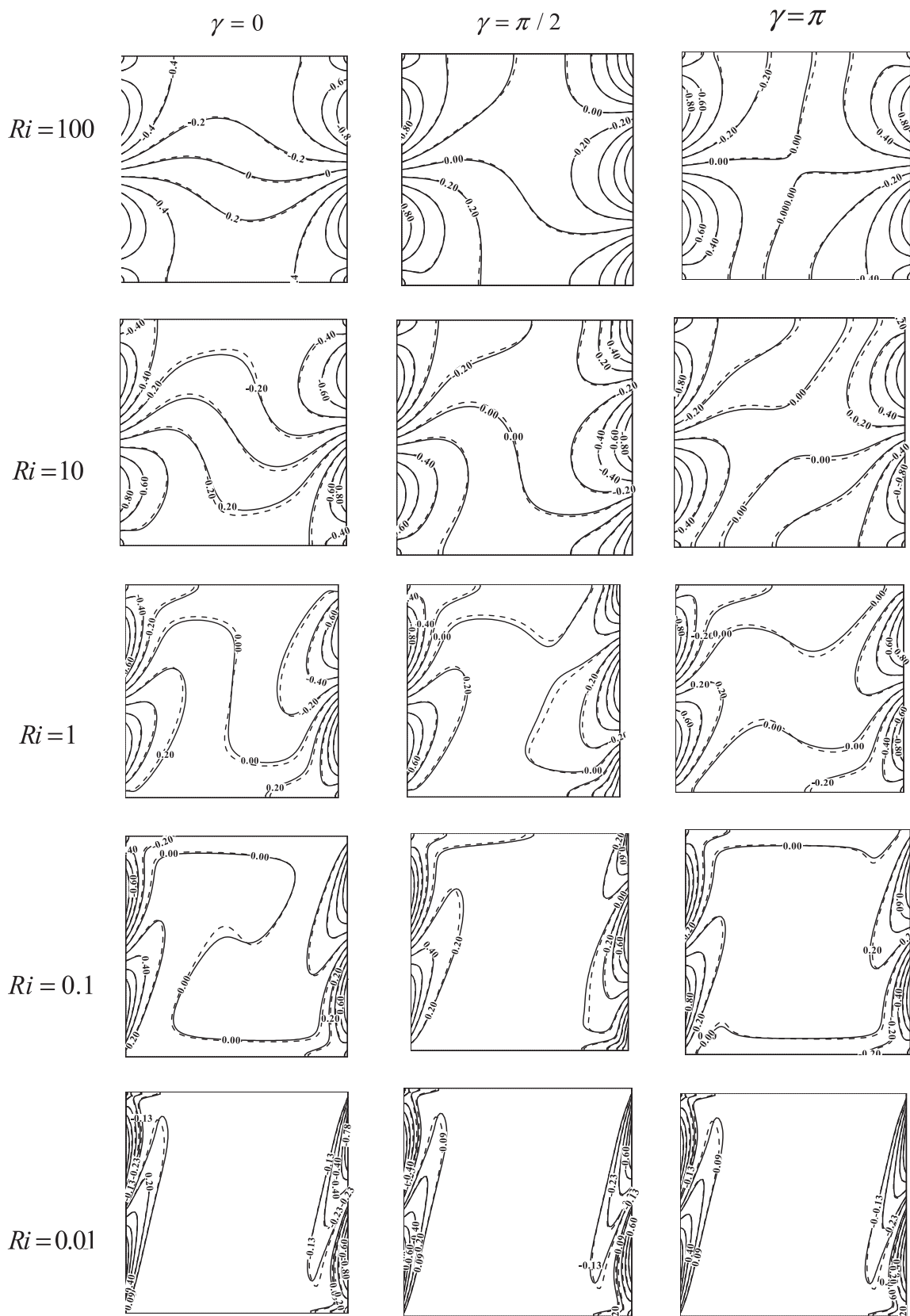*4.2. Study of dimensionless temperature at the center of the cavity*

Fig. 7 shows the dimensionless temperature in horizontal direction in the middle of cavity for Richardson number of 0.01, 0.1,

1, 10 and 100, the temperature phase deviation of $\gamma = 0$, $\gamma = \pi/2$, $\gamma = 3\pi/4$, and $\gamma = \pi$, and the volume fraction of 0.04. As can be seen, by decreasing the Richardson number for all temperature phase deviations which are considered, the maximum dimensionless temperature increases due to the Reynolds number increases and so the forced convection is dominant and the temperature gradient near the side walls increases. Since the phase deviation of the left wall is zero, temperature in the middle of the left wall becomes zero and after that the wall temperature increases abruptly. Also when the Richardson number decreases, the maximum dimensionless temperature occurs close to the walls. Because in low Richardson numbers a thinner boundary layer and a stronger temperature gradient occur, which leads to an increase in temperature gradient and approaches the maximum temperature to the wall.

4.3. Investigation of local Nusselt number on side walls

In Fig. 8 the variations of the local Nusselt number along the left and right walls of the cavity are illustrated in Richardson

Figure 5   The stream lines for different temperature phase deviations and Richardson numbers for nanofluid in $\varphi = 0.04$.

Figure 6 The isothermal lines in different temperature phase deviations and Richardson numbers for pure fluid (- -) and nanofluid (-) in $\varphi = 0.06$.
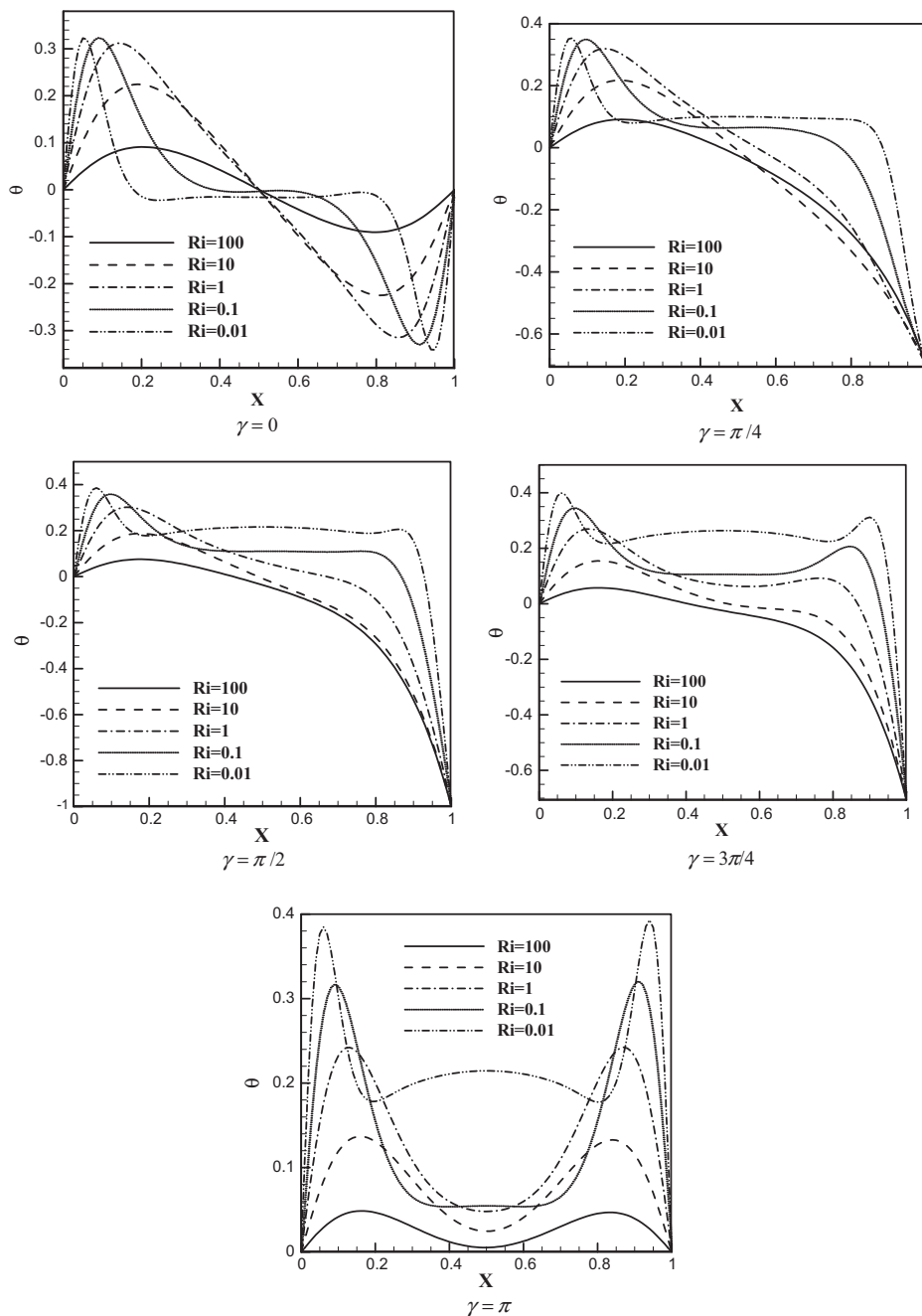
Figure 7 Dimensionless temperature in horizontal direction in the middle of cavity for different Richardson numbers and temperature phase deviations in $\varphi = 0.04$.

numbers 0.01, 0.1, 1, 10 and 100, and the temperature phases deviation $\gamma = 0$, $\gamma = \pi/2$, $\gamma = 3\pi/4$ and $\gamma = \pi$, and $\varphi = 0.04$. In this figure it is evident that the effect of the temperature phase deviation change on local Nusselt number of the right wall is more than the left wall. Because the temperature phase deviation change only occurs on the right wall. In terms of heat transfer, the side walls are divided into two distinct parts which are named hot and cold areas due to the temperature phase deviation. For the left side wall because of the zero phase deviation, the wall is divided into just two parts: hot (lower half of the wall) and cold (upper half of the wall). In Richardson numbers 1, 10 and 100, by increasing the temperature phase deviation, the heat transfer increases in the hot part of the wall. With an increase in the Richardson number, the effect of the raising phase deviation on heat transfer of the cold part of the wall reduces, so that the increasing phase deviation in $Ri = 100$ has little effect on heat transfer in the cold area. When the Richardson number decreases this process is reversed gradually in a way that in the Richardson numbers less than one, the heat transfer from the hot wall reduces while
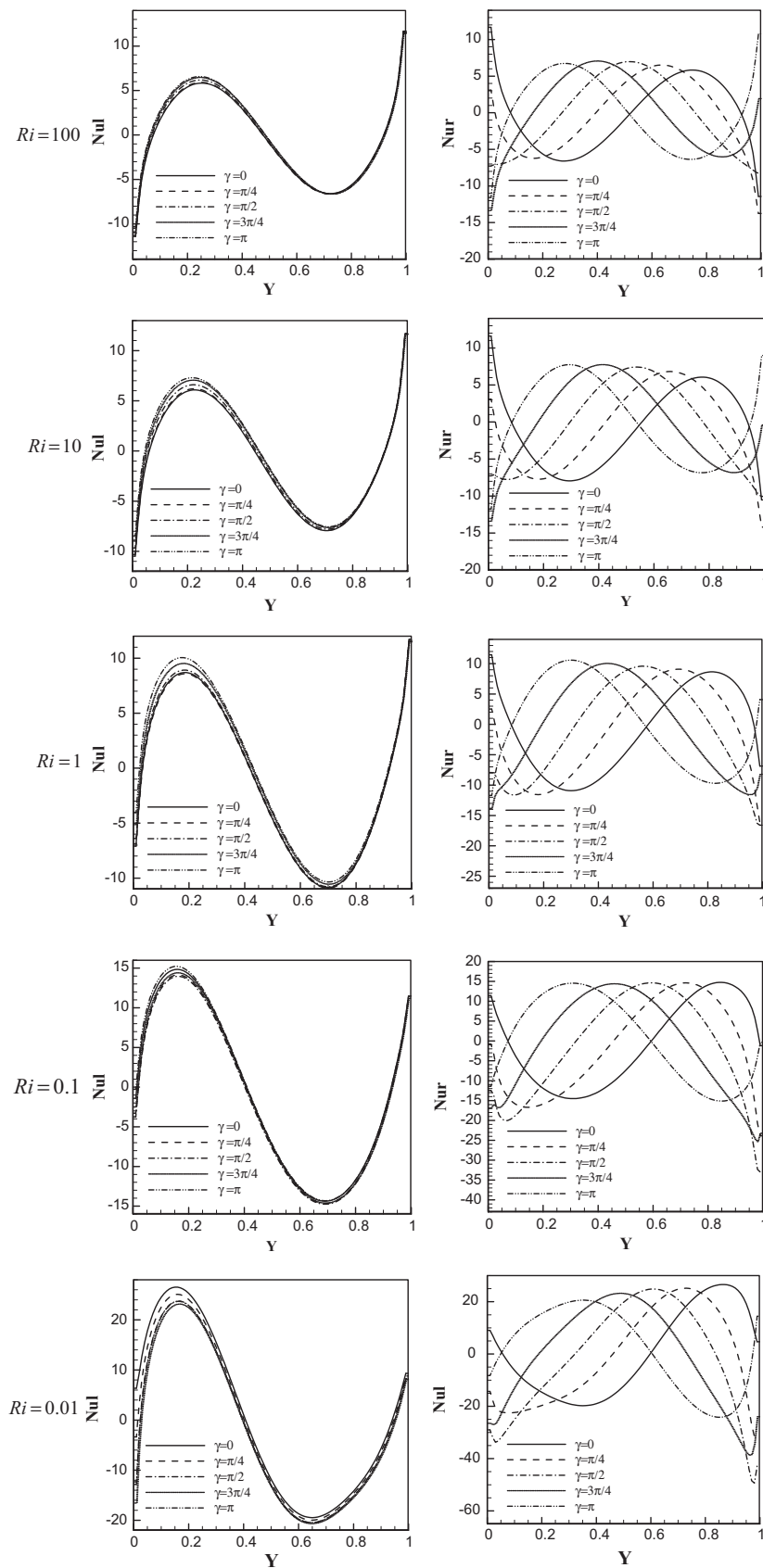
Figure 8 The local Nusselt number change along the left and right walls for different Richardson numbers and phase deviations in $\varphi = 0.04$.

the heat transfer to the cold area of the wall increases. By reducing the Richardson number, the maximum heat transfer of the hot and cold areas of the wall, increases.

4.4. Study of the average Nusselt number

In Fig. 9 the average Nusselt number along the right wall of the cavity is indicated in Richardson numbers 0.01, 0.1, 1, 10 and 100, the temperature phases deviation $\gamma = 0$, $\gamma = \pi/2$, $\gamma = 3\pi/4$ and $\gamma = \pi$, and the volume fraction of nanoparticles

0 to 0.06. As can be seen, in all Richardson numbers and temperature phase deviations, by increasing the volume fraction of nanoparticles, the heat transfer rate improves. Also for all Richardson numbers in constant volume fraction of nanoparticles, by increasing the temperature phase deviation from 0 to $\pi/2$, the average Nusselt number and thus the heat transfer rate increase. Also by increasing the temperature phase deviation from $\pi/2$ to π, the average Nusselt number and the heat transfer rate decrease. The maximum Nusselt number and heat transfer rate for all Richardson number occur in $\gamma = \pi/2$ due to the motion of the upper and bottom walls.
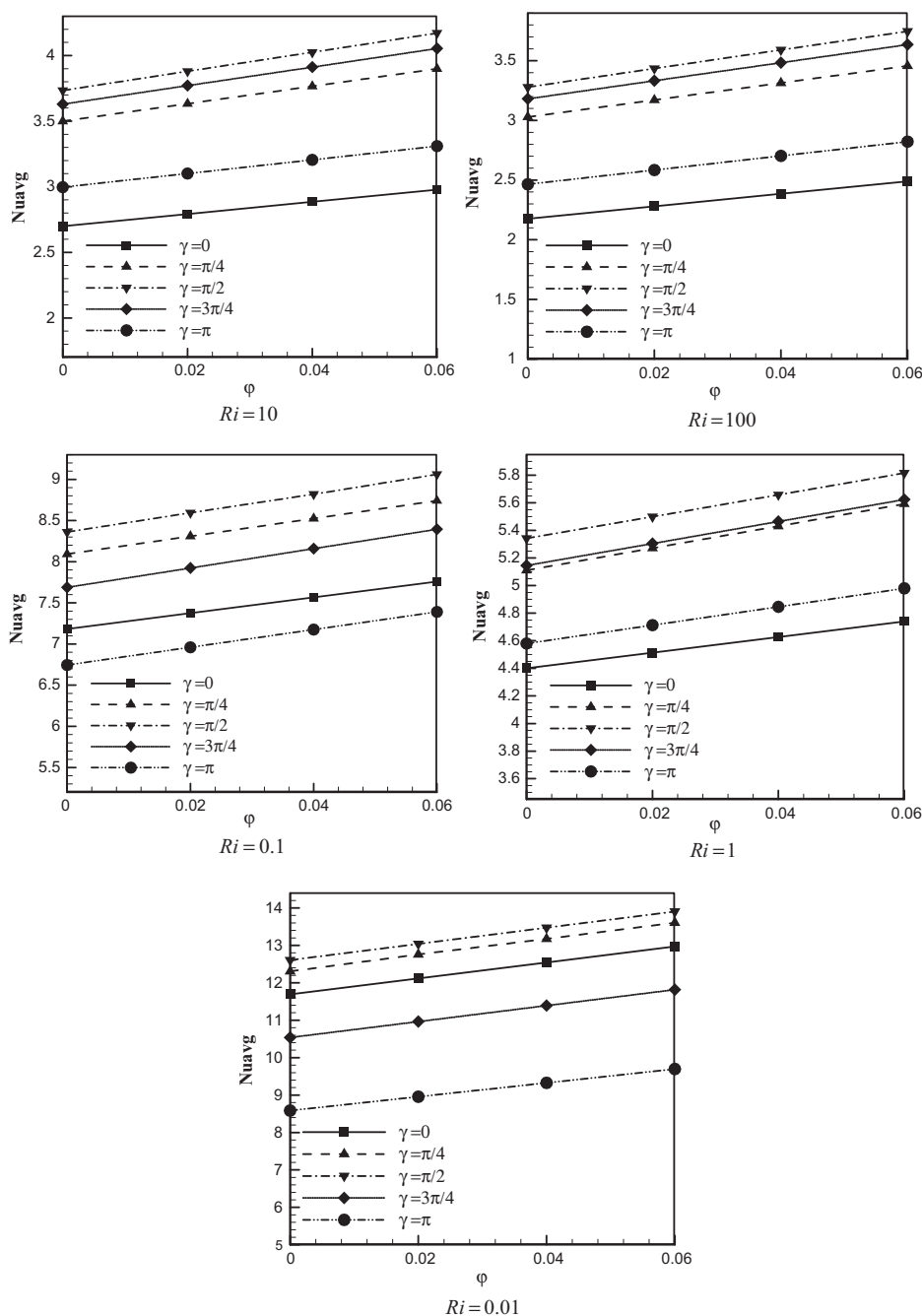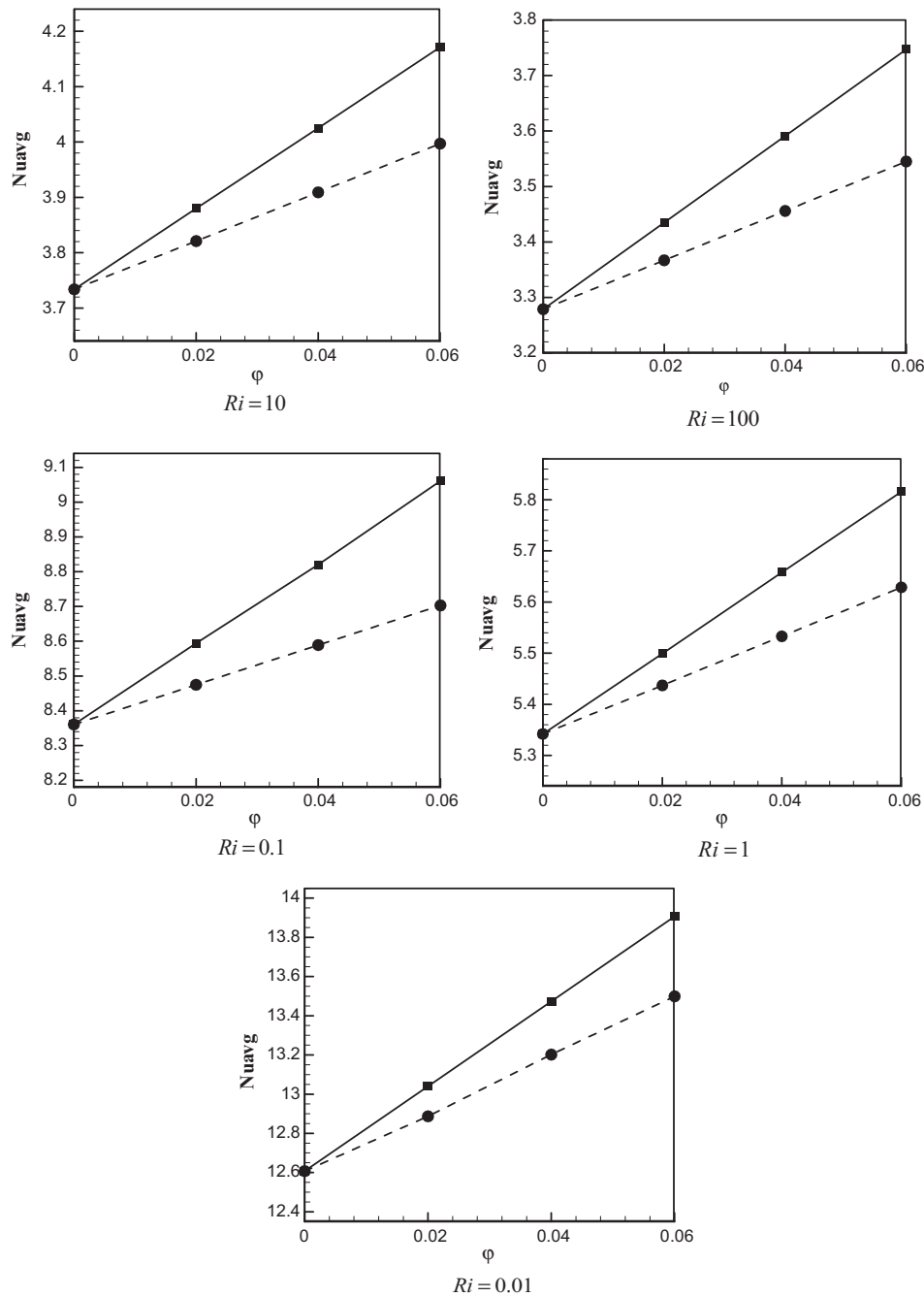

Figure 9 The average Nusselt number in terms of the volume fraction of nanoparticles along the right wall in different Richardson numbers and temperature phase deviations.

4.5. Comparing the average Nusselt number for constant and variable properties models of nanofluids

In Fig. 10, the variations of the average Nusselt number for constant and variable properties models of nanofluids are shown in Richardson numbers 0.01, 0.1, 1, 10 and 100, the temperature phase deviation $\gamma = \pi/2$ and the volume fraction of nanoparticles 0 to 0.06. As already mentioned for constant properties, the Brinkman model [47] for viscosity and the Maxwell model [48] for thermal conductivity coefficient are applied and for variable properties, the Brinkman model [47] for viscosity and Patel et al's model [38] for thermal conductivity coefficient are used. As can be seen in Fig. 10, for all Richardson numbers, the obtained Nusselt number in constant properties model is greater than the variable properties model due to higher estimation of the thermal conductivity coefficient in constant properties model. It should be noted that for both models, the average Nusselt number increases by decreasing Richardson number in which the heat transfer rate in the cavity increases.

Figure 10 Variations of the average Nusselt number for constant (-) and variable (- - -) properties models of nanofluids in different Richardson numbers and $\gamma = \pi/2$, and the volume fraction of nanoparticles 0 to 0.06.

5. Conclusion

In this study, mixed convection heat transfer of water-Cu nanofluid in a double lid-driven cavity is examined by use of the lattice Boltzmann method. The double lid-driven are adiabatic and the side walls have sinusoidal temperature distribution. Simulations have been done at constant Grashof number 100 and different Richardson numbers, phase deviation, the solid volume fraction from and the Prandtl number of 6.57. Based on the numerical results, it was observed that:

- In low Richardson numbers, the temperature phase deviation change has no effect on the flow pattern, but by increasing it, the effect of the temperature phase deviation change on the flow pattern is evident.
- By reducing the Richardson number, a severe temperature gradient along the side walls is taken place and the Nusselt number and heat transfer increase.
- For all Richardson numbers and in all temperature phase deviations, by increasing the volume fraction of nanoparticles up to 6%, the heat transfer rate improves.
- By reducing the Richardson number for all temperature phase deviations, the maximum dimensionless temperature increases.
- By reducing the Richardson number, the maximum dimensionless temperature is occurred near the walls.
- The maximum Nusselt number and heat transfer rate for all Richardson number are occurred in $\gamma = \pi/2$ due to the motion of the upper and bottom walls.
- For all Richardson numbers the obtained Nusselt number in constant properties model is greater than the variable properties model.

6. List of symbols

c_i	discreet velocity of Boltzmann grid
c_p (J/kg K)	specific heat at constant pressure
c_s	sound speed
d_f (nm)	diameter of water molecules
d_p (nm)	nanoparticle diameter
F (kg ms^{-2})	buoyancy force
f_i	the distribution function
f_i^{eq}	the local equilibrium distribution function
g	the gravitational acceleration
g_i	temperature distribution function
g_i^{eq}	the local equilibrium distribution function of temperature
G (m/s^2)	acceleration of gravity
Gr	Grashof Number, $\frac{g\beta\Delta TH}{v^2}$
H (m)	the height of cavity
k_B (J/K)	Boltzmann constant
k (W/m K)	conduction heat transfer coefficient
Nu_{avg}	the average Nusselt number
Ma	mach number
p (N/m^2)	pressure
P	dimensionless pressure
Pr	Prandtl number
Re	Reynolds number
Ra	Rayleigh number
Ri	Richardson number

T (K)	temperature
U (m/s)	velocity component in the direction of x
V (m/s)	velocity component in the direction of y
U	dimensionless velocity component in the direction of X
V	dimensionless velocity component in the direction of Y
Greek symbols	
α (m^2/s)	thermal diffusivity
β (1/K)	coefficient of thermal expansion
μ (kg/ms)	viscosity
Y (m^2/s)	kinematic viscosity
θ	dimensionless temperature
ρ (kg/m^3)	density
φ	volume fraction of nanoparticles
γ	temperature phase deviation
τ_c	relaxation time of the flow field
τ_v	relaxation time of the temperature field
ω_i	the weight function of the ith direction
Footnotes	
Average	avg
Cold	c
Fluid	f
Hot	h
Nanofluid	nf
Nanoparticle	p

References

[1] L.A.B. Pilkington, Review lecture: the float glass process, Proc. Roy. Soc. Lond. A314 (1969) 1–25.

[2] J. Imberger, P.F. Hamblin, Dynamics of lakes, reservoirs, and cooling ponds, Ann. Rev. Fluid Mech. 14 (1982) 153–187.

[3] D. Lourdu Immaculate, R. Muthuraj, R.K. Selvi, S. Srinivas, Anant Kant Shukla, The influence of thermophoretic particle deposition on fully developed MHD mixed convective flow in a vertical channel with thermal-diffusion and diffusion-thermo effects, Ain Shams Eng. J. 6 (2015) 671–681.

[4] R. Seshadri, Sh.R. Munjam, Mixed convection flow due to a vertical plate in the presence of heat source and chemical reaction, Ain Shams Eng. J. (2015).

[5] D. Srinivasacharya, B. Mallikarjuna, R. Bhuvanavijaya, Soret and Dufour effects on mixed convection along a vertical wavy surface in a porous medium with variable properties, Ain Shams Eng. J. 6 (2015) 553–564.

[6] A. Saha, T. Malik, Mixed convection flow and heat transfer through a horizontal channel with surface mounted obstacles, J. Enhanced Heat Transfer 19 (2012) 313–329.

[7] S.H. Hussain, Q.R. Abd-Amer, Mixed convection heat transfer flow of air inside a sinusoidal corrugated cavity with a heat conducting horizontal circular cylinder, J. Enhanced Heat Transfer 18 (2011) 433–447.

[8] K. Bhattacharyya, S. Mukhopadhyay, G.C. Layek, Similarity solution of mixed convective boundary layer slip flow over a vertical plate, Ain Shams Eng. J. 4 (2013) 299–305.

[9] P. Shiang-Wuu, W. Horng-Wen, Heat transfer enhancement for turbulent mixed convection in reciprocating channel by various rib installation, J. Enhanced Heat Transfer 20 (2013) 95–114.

[10] T. Hayat, M. Bilal Ashraf, H.H. Alsulami, On mixed convection flow of Jeffrey fluid over an inclined stretching surface with thermal radiation, Heat Transfer Res. 46 (2015) 515–539.

[11] M.A. Teamah, W.M. El-Maghlany, Numerical simulation of double-diffusive convective flow in differentially heated

rectangular enclosure with insulated moving lid on top, Int. J. Therm. Sci. 49 (9) (2010) 1625–1638.

[12] M. Teamah, M. Sorour, W.M. El-Maghlany, Amr. Afifi, Numerical simulation of double diffusive laminar mixed convection in shallow inclined cavities with moving lid, Alexandria Eng. J. 52 (3) (2013) 227–239.

[13] M.A.R. Sharif, Laminar mixed convection in shallow inclined driven cavities with hot moving lid on top and cooled from bottom, Appl. Therm. Eng. 27 (2007) 1036–1042.

[14] R.K. Tiwari, M.K. Das, Heat transfer augmentation in a two-sided lid-driven differentially heated square cavity utilizing nanofluids, Int. J. Heat Mass Transfer 50 (2007) 2002–2018.

[15] M. Muthtamilselvan, P. Kandaswamy, J. Lee, Heat transfer enhancement of copper–water nanofluids in a lid-driven enclosure, Commun. Nonlinear Sci. Numer. Simulat. 15 (2010) 1501–1510.

[16] A. Arefmanesh, M. Mahmoodi, Effects of uncertainties of viscosity models for Al_2O_3–water nanofluid on mixed convection numerical simulations, Int. J. Therm. Sci. 50 (2011) 1706–1719.

[17] S. Mazrouei Sebdani, M. Mahmoodi, S.M. Hashemi, Effect of nanofluid variable properties on mixed convection in a square cavity, Int. J. Therm. Sci. 52 (2012) 112–126.

[18] M. Hemmat Esfe, A.H. Refahi, H. Teimouri, M.J. Noroozi, M. Afrand, A. Karimiopour, Mixed convection fluid flow and heat transfer of the Al_2O_3-water nanofluid with variable properties in a cavity with an inside quadrilateral obstacle, Heat Transfer Res. 46 (2015) 465–482.

[19] M. Hemmat Esfe, M. Akbari, D. Toghraei Semiromi, A. Karimiopour, M. Afrand, Effect of nanofluid variable properties on mixed convection flow and heat transfer in an inclined two-sided lid-driven cavity with sinusoidal heating on side walls, Heat Transfer Res. 45 (2014) 409–432.

[20] M. Hemmat Esfe, S.S. Mirtalebi Esforjani, M. Akbari, A. Karimiopour, Mixed-convection flow in a lid-driven square cavity with a nanofluid with variable properties: effect of the nanoparticle diameter and of the position of a hot obstacle, Heat Transfer Res. 45 (2014) 563–578.

[21] S. Shehzad, F.E. Alsaadi, T. Hayat, S.J. Monaquel, MHD mixed convection flow of Thixo tropic fluid with thermal radiation, Heat Transfer Res. 45 (2014) 569–676.

[22] M. Hemmat Esfe, S. Niazi, S.S. Mirtalebi Esforjani, M. Akbari, Mixed convection flow and heat transfer in a ventilated inclined cavity containing hot obstacles subjected to a nanofluid, Heat Transfer Res. 45 (2014) 309–338.

[23] M. Hemmat Esfe, S.S. Mirtalebi Esforjani, M. Akbari, Mixed convection flow and heat transfer in a lid-driven cavity subjected to nanofluid: effect of temperature, concentration and cavity inclination angles, Heat Transfer Res. 45 (2014) 453–470.

[24] M.R. Heydari, M. Hemmat Esfe, M.H. Hajmohammad, M. Akbari, S.S. Mirtalebi Esforjani, Mixed convection heat transfer in double lid-driven inclined square enclosure subjected to Cu-water nanofluid with particle diameter of 90 nm, Heat Transfer Res. 45 (2014) 75–95.

[25] M. Hemmat Esfe, S.S. Mirtalebi Esforjani, M. Akbari, M.H. Hajmohammad, Numerical simulation of mixed convection in a SiO_2-water nanofluid in a two sided lid-driven square enclosure with sinusoidal boundary conditions on the wall, Heat Transfer Res. 45 (2014) 677–700.

[26] M.R. Faridzadeh, D. Toghraei Semiromi, A. Niroomand, Analysis of laminar mixed convection in an inclined square cavity with a nanofluid by using an artificial neural network, Heat Transfer Res. 45 (2014) 361–390.

[27] F. Bazdadi-Tehrani, A. Safakish, Mixed-convection and thermal radiation heat transfer in a three dimensional asymmetrically heated vertical channel, Heat Transfer Res. 45 (2014) 541–561.

[28] M.A. Teamah, W.M. El-Maghlany, Augmentation of natural convective heat transfer in square cavity by utilizing nanofluids

in the presence of magnetic field and uniform heat generation/absorption, Int. J. Therm. Sci. 58 (2012) 130–142.

[29] S. Nadeem, Hina Sadaf, M. Adil Sadiq, Analysis of nanoparticles on peristaltic flow of Prandtl fluid model in an endoscopy, Curr. Nanosci. 10 (5) (2014) 709–721.

[30] S. Nadeem, Hina. Sadaf, Theoretical analysis of Cu-blood nanofluid for metachronal wave of cilia motion in a curved channel, Trans. Nanobiosci. 14 (4) (2015) 447–454.

[31] S. Nadeem, Hina Sadaf, Noreen Sher Akbar, Effects of nanoparticles on the peristaltic motion of tangent hyperbolic fluid model in an annulus, Alexandria Eng. J. 54 (4) (2015) 843–851.

[32] S. Nadeem, Hina. Sadaf, Trapping study of nanofluids in an annulus with cilia, AIP Adv. 5 (12) (2015) 127204.

[33] P. Sudarsana Reddy, Ali J. Chamkha, Influence of size, shape, type of nanoparticles, type and temperature of the base fluid on natural convection MHD of nanofluids, Alexandria Eng. J. 55 (1) (2016) 331–341.

[34] Khan Md. Rabbi, Sourav Saha, Satyajit Mojumder, M.M. Rahman, R. Saidur, Talaat A. Ibrahim, Numerical investigation of pure mixed convection in a ferrofluid-filled lid-driven cavity for different heater configurations, Alexandria Eng. J. 55 (1) (2016) 127–139.

[35] Ahmed Kadhim Hussein, Salam Hadi Hussain, Heatline visualization of natural convection heat transfer in an inclined wavy cavities filled with nanofluids and subjected to a discrete isoflux heating from its left sidewall, Alexandria Eng. J. 55 (1) (2016) 169–186.

[36] O. Pourmehran, M. Rahimi-Gorji, M. Gorji-Bandpy, D.D. Ganji, Analytical investigation of squeezing unsteady nanofluid flow between parallel plates by LSM and CM, Alexandria Eng. J. 54 (1) (2015) 17–26.

[37] H. Nemati, M. Farhadi, K. Sedighi, E. Fattahi, Lattice Boltzmann simulation of nanofluid in lid-driven cavity, Int. Commun. Heat Mass Trans. 37 (2010) 1528–1534.

[38] A.A. Rabienatajdarzi, M. Farhadi, K. Sedighi, E. Fattahi, H. Nemati, Mixed convection simulation of inclined lid driven cavity using lattice Boltzmann method, Trans. Mech. Eng. 35 (2010) 73–83.

[39] A. Karimpour, A.H. Nezhad, A. D'Orazia, E. Shirani, The effects of inclination angle and Prantel number on the mixed convection in the inclined lid driven cavity using lattice boltzmann method, J. Theoret. Appl. Mech. 51 (2013) 447–462.

[40] J. Alinejad, J. Abolfazli Esfahani, Lattice Boltzmann simulation of forced convection over an electronic board with multiple obstacles, Heat Transfer Res. 45 (2014) 241–262.

[41] H. Sajjadi, G.H.R. Kefayati, MHD Turbulent and laminar natural convection in a square Cavity utilizing Lattice Boltzmann method, Heat Transfer – Asian Res. (2015).

[42] B. Gera, R.K. Singh, Lattice Boltzmann method based simulation of natural convection in partially open enclosure, Heat Transfer – Asian Res. 44 (2015) 154–171.

[43] H. Sajjadi, S. Zafariyan, Lattice Boltzmann simulation of natural convection in a square cavity with linearly heated wall (s), Heat Transfer – Asian Res. 44 (2015) 450–467.

[44] H.R. Ashorynejad, K. Sedighi, M. Farhadi, E. Fattahi, Simulating magnetohydrodynamic natural convection flow in a horizontal cylindrical annulus using the lattice Boltzmann method, Heat Transfer – Asian Res. 41 (2012) 468–483.

[45] M. Jafari, M. Farhadi, S. Akbarzade, M. Ebrahimi, Lattice Boltzmann simulation of natural convection heat transfer of SWCNT-nanofluid in an open enclosure, Ain Shams Eng. J. (2015).

[46] H.F. Oztop, E. Abu-Nada, Numerical study of natural convection in partially heated rectangular enclosures filled with nanofluids, Int. J. Heat Fluid Flow 29 (2008) 1326–1336.

[47] H. Brinkman, The viscosity of concentrated suspensions and solutions, J. Chem. Phys. 20 (1952) 571–581.

[48] J. Maxwell, A Treatise on Electricity and Magnetism Unabridged, Dover, 1954.

[49] H.E. Patel, T. Sundararajan, T. Pradeep, A. Dasgupta, N. Dasgupta, S.K. Das, A micro-convection model for thermal conductivity of nanofluids, J. Phys. 65 (2005) 863–869.

[50] A.A. Mohamad, R. Viskanta, Stability of lid-driven shallow cavity heat from below, Int. J. Heat Mass Transf. 32 (1989) 2155–2166.

[51] S. Sivasankaran, V. Sivakumar, P. Prakash, Numerical study on mixed convection in a lid-driven cavity with non-uniform heating on both sidewalls, Int. J. Heat Mass Transf. 53 (2010) 4304–4315.

[52] E. Abu-Nada, A.J. Chamkha, Mixed convection flow in a lid-driven inclined square enclosure filled with a nanofluid, Eur. J. Mech. B Fluids 29 (2010) 472–482.